The neonatal microenvironment programs innate γδ T cells through the transcription factor STAT5

Darshana Kadekar,[1] Rasmus Agerholm,[1] John Rizk,[1] Heidi A. Neubauer,[2] Tobias Suske,[2] Barbara Maurer,[2] Monica Torrellas Viñals,[1] Elena M. Comelli,[3,4] Amel Taibi,[3] Richard Moriggl,[2] and Vasileios Bekiaris[1]

[1]Department of Health Technology, Technical University of Denmark, Kongens Lyngby, Denmark. [2]Institute of Animal Breeding and Genetics, University of Veterinary Medicine Vienna, Vienna, Austria. [3]Department of Nutritional Sciences and [4]Department of Nutritional Sciences and Joannah and Brian Lawson Centre for Child Nutrition, Faculty of Medicine, University of Toronto, Toronto, Ontario, Canada.

IL-17–producing RORγt$^+$ γδ T cells (γδT17 cells) are innate lymphocytes that participate in type 3 immune responses during infection and inflammation. Herein, we show that γδT17 cells rapidly proliferate within neonatal lymph nodes and gut, where, upon entry, they upregulate T-bet and coexpress IL-17, IL-22, and IFN-γ in a STAT3- and retinoic acid–dependent manner. Neonatal expansion was halted in mice conditionally deficient in STAT5, and its loss resulted in γδT17 cell depletion from all adult organs. Hyperactive STAT5 mutant mice showed that the STAT5A homolog had a dominant role over STAT5B in promoting γδT17 cell expansion and downregulating gut-associated T-bet. In contrast, STAT5B preferentially expanded IFN-γ–producing γδ populations, implying a previously unknown differential role of STAT5 gene products in lymphocyte lineage regulation. Importantly, mice lacking γδT17 cells as a result of STAT5 deficiency displayed a profound resistance to experimental autoimmune encephalomyelitis. Our data identify that the neonatal microenvironment in combination with STAT5 is critical for post-thymic γδT17 development and tissue-specific imprinting, which is essential for infection and autoimmunity.

Introduction

IL-17–producing γδ T cells (γδT17 cells) are one of the major type 3 innate lymphocytes in the mouse, occupying the skin and most mucosal surfaces as well as secondary lymphoid organs. Their ability to constitutively produce IL-17 and to respond rapidly to cytokines like IL-7, IL-23, and IL-1β renders them a critical part of innate immunity to infections (1, 2) but also makes them highly pathogenic in a number of inflammatory models (3–5). Thus, both experimental autoimmune encephalomyelitis (EAE) and imiquimod-induced psoriasis require the presence of functional γδT17 cells (3, 5). Similarly, tumor models have shown that γδT17 cells can have either protective (6) or pathogenic (7) roles depending on the nature of the cancer. In humans, although a unique innate γδT17 cell population has not yet been characterized, many groups have identified IL-17–producing γδ T cells in association with various disease states (6, 8).

Genetic murine studies have shown that γδT17 cells develop in the embryonic thymus in a stepwise fashion, initially involving escape of epithelial selection (9), followed by the upregulation of a number of transcription factors, such as RORγt, SOX13, and cMAF, that regulate lineage commitment, specification, and functional maturation (10, 11). Although T cell receptor (TCR) signaling is necessary for γδT17 cell development (12), experimental evidence based on hypomorphic CD3 mice and anti-CD3/TCR antibody administration suggested that only weak TCR signals are required (13, 14). In addition, a recent study showed that TCR signaling is not important for lineage specification but is important for transition into the early immature stage (15). γδT17 cell generation is restricted to the embryonic and neonatal thymus (16), with the bone marrow displaying low capacity to produce these cells (17).

STAT transcription factors act downstream of cytokine and growth factor receptors to regulate a plethora of key biological processes, including lymphocyte development and function (18). STAT5 is encoded by 2 genes, *Stat5a* and *Stat5b*, giving rise to 2 highly homologous proteins with largely overlapping functions in mediating transcription of target genes, although STAT5B has a more dominant role in lymphoid cells as well as in cancer progression (19, 20). Mice deficient in both STAT5A and STAT5B have increased perinatal mortality and lack or display a severe reduction in many lymphocytic populations, such as αβ T cells, γδ T cells, regulatory CD4$^+$ T cells (Tregs), natural killer (NK) T cells, NK cells, and also B cells (21–23). Although mice deficient in either STAT5A or STAT5B show hampered development and function of a few major lymphocyte subsets, their phenotype is milder than that seen with combined loss of the 2 isoforms (19, 24, 25). However, there are currently no mechanistic data regarding their individual contribution in γδ T cell biology. One of the suggested mechanisms for the dependence of developing γδ T cell progenitors on STAT5 is its ability to induce TCRγ rearrangements, due to 3 highly interspecies-conserved inverted-repeat STAT5 consensus sites within the *Tcrg* locus (26).

In humans, *STAT5*-associated loss-of-function mutations are predominantly restricted to STAT5B, and these culminate in growth failure due to impaired growth hormone receptor signaling, as well as immunodeficiency, metabolic dysregulation, and autoimmune disorders as a result of Treg deficiency (27–29). In contrast, *STAT5B* gain-of-function (GOF) mutations strongly correlate with mature T cell neoplasms (30) and have also been found

Authorship note: DK, RA, and JR contributed equally to this work.
Conflict of interest: The authors have declared that no conflict of interest exists.

Submitted: June 21, 2019; **Accepted:** January 29, 2020; **Published:** April 13, 2020.
Reference information: *J Clin Invest*. 2020;130(5):2496–2508.
https://doi.org/10.1172/JCI131241.

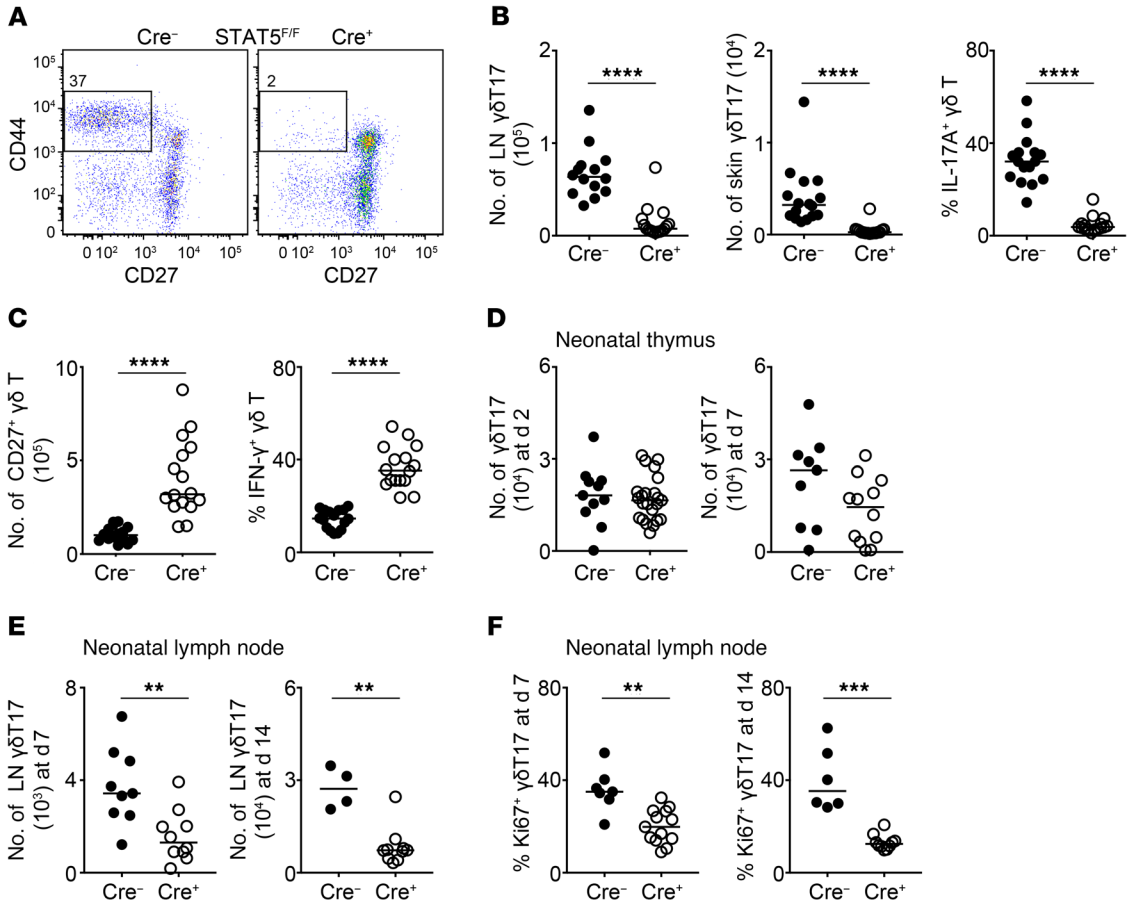

Figure 1. STAT5 is necessary for the neonatal expansion of γδT17 cells. Flow cytometric analysis of γδ T cells in RORγt^{CRE}-STAT5$^{F/F}$ (Cre$^+$) and littermate control mice (Cre$^-$). In graphs, each symbol represents a mouse, and lines represent the median. $^{**}P < 0.01$, $^{***}P < 0.001$, $^{****}P < 0.0001$ using Mann-Whitney test. (**A**) Expression of CD27 and CD44 in order to identify CD27$^-$CD44$^+$ γδT17 cells in the LN. Numbers indicate percentage of CD27$^-$CD44$^+$ within the γδ T cell compartment. (**B**) Numbers of γδT17 cells in the LN (staining as in **A**) and skin and frequency of IL-17A–producing cells within the LN γδ T cell compartment. In the skin, γδT17 cells were identified as CD45$^+$CD3^{lo}Vγ5$^-$TCRβ$^-$TCRγδ$^+$CCR6$^+$. (**C**) Numbers of CD27$^+$ γδ T cells in the LN and frequency of IFN-γ–producing cells within the LN γδ T cell compartment. (**D**) Numbers of CD27$^-$CD44$^+$ γδT17 cells in 2- and 7-day-old thymi. (**E**) Numbers of CD27$^-$CD44$^+$ γδT17 cells in 7- and 14-day-old LN. (**F**) Frequency of Ki67$^+$RORγt$^+$ or Ki67$^+$CCR6$^+$ cells within the CD44$^+$TCRγδ$^+$ compartment in 7- and 14-day-old LN. (**A**–**C**) n = 14–16 mice, 5 experiments; (**D**) n = 11 (d2) and 9 (d7) Cre$^-$ mice and 23 (d2) and 12 (d7) Cre$^+$ mice, 3 experiments; (**E**) n = 9 (d7) and 4 (d14) Cre$^-$ mice and 10 (d7) and 10 (d14) Cre$^+$ mice, 3 experiments; (**F**) n = 7 (d7) and 6 (d14) Cre$^-$ mice and 13 (d7) and 10 (d14) Cre$^+$ mice, 3 experiments.

in patients with neutrophilia or eosinophilia (31, 32). In particular, the recurrent N642H GOF missense mutation within the Src homology 2 (SH2) domain of STAT5B results in enhanced and prolonged tyrosine phosphorylation (pY) in response to low doses of cytokines or growth factors, and is associated with poorer patient prognosis and increased risk of relapse (30, 33, 34). Interestingly, *STAT5B* GOF mutations are relatively frequent in aggressive γδ T cell lymphoma subtypes, such as hepatosplenic T cell lymphoma (35), monomorphic epitheliotropic intestinal T cell lymphoma (36, 37), and primary cutaneous γδ T cell lymphoma (37). Notably, approximately 20% of identified N642H mutations occur in γδ T cell–derived lymphomas (20).

Herein, we show that STAT5 is critically required for the progression and expansion of γδT17 cells through neonatal life in the intestine and periphery. We provide evidence that intestinal γδT17 cells upregulate T-bet upon entry into the lamina propria after birth and coexpress the cytokines IL-17, IL-22, and IFN-γ in a mechanism dependent on STAT3 and retinoic acid. Furthermore, loss of γδT17 cells due to STAT5 deficiency results in resistance to EAE in adult mice. Importantly, we show that STAT5A promotes γδT17 cell expansion and downregulates intestinal T-bet, favoring a type 17 program, whereas STAT5B favors IFN-γ–producing γδ populations and increases intestinal T-bet expression. Collectively, our data suggest that neonatal life is a critical window of development and tissue specification for γδT17 cells, and that this process is tightly regulated by STAT5.

Results

STAT5 regulates the neonatal expansion of γδT17 cells. In order to test the importance of STAT5 in RORγt-expressing γδ T cells, we crossed *Rorc*-Cre (RORγt^{CRE}) mice (38) with mice floxed for both *Stat5a* and *Stat5b* (RORγt^{CRE}-STAT5$^{F/F}$) (39) and analyzed the numbers of lymph node (LN) and skin γδT17 cells. We found that compared with littermate controls (Cre$^-$), RORγt^{CRE}-STAT5$^{F/F}$ mice (Cre$^+$) contained severely reduced numbers of γδT17 cells defined phenotypically as CD27$^-$CD44$^+$ in the LN and CCR6$^+$CD3$^+$ in the skin (Figure 1, A and B). This was confirmed by the near-complete lack of IL-17–expressing γδ T cells in the LN (Figure 1B). Deficiency

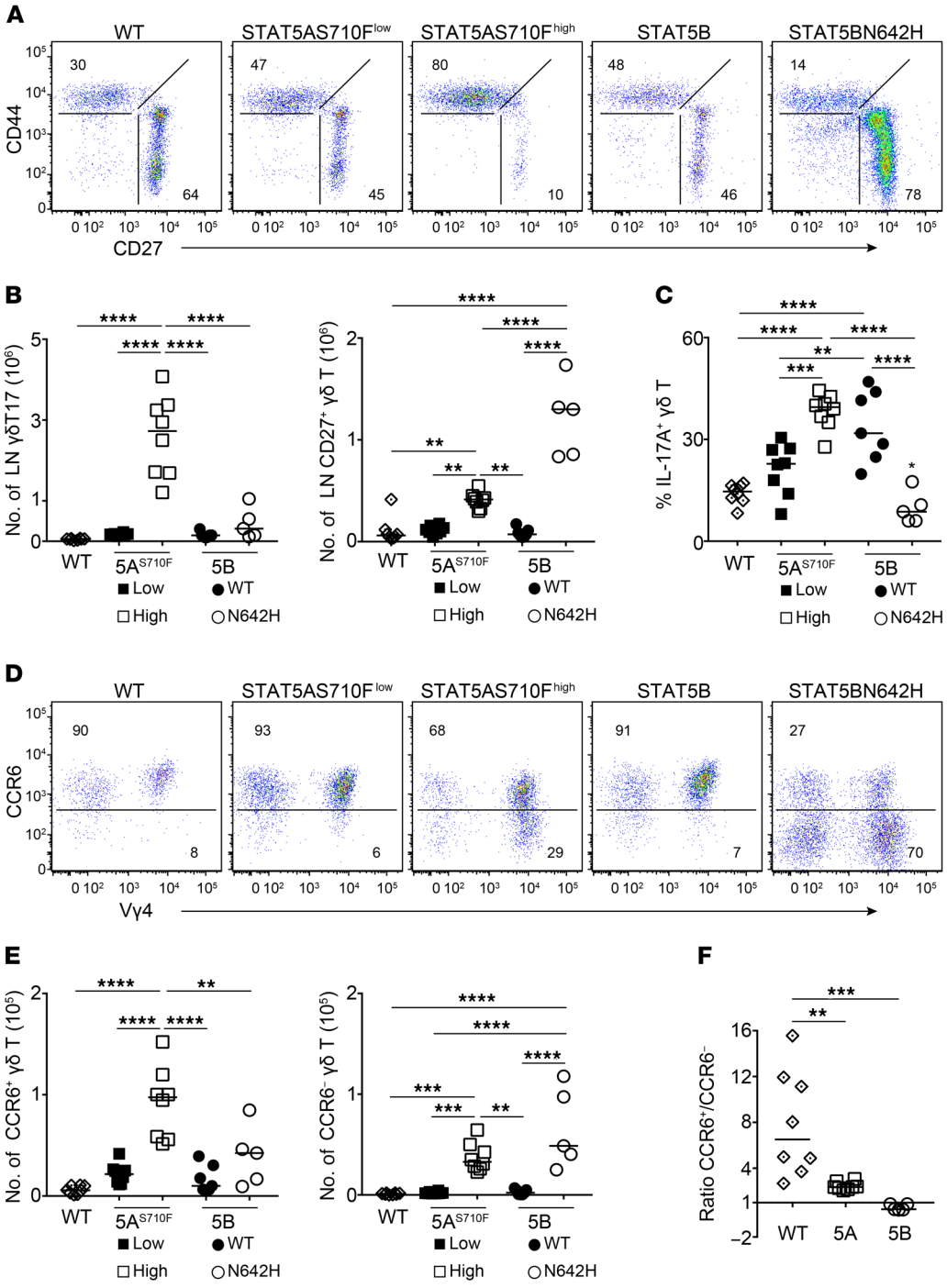

Figure 2. Differential impact of STAT5A and STAT5B on γδT17 and CD27⁺ γδ T cells. Flow cytometric analysis of γδ T cells in mice that either are wild type or constitutively express under the *Vav1* promoter one of the following forms of STAT5: low (STAT5AS710F^{low}) or high (STAT5AS710F^{high}) copy number of the hyperactive STAT5A S710F mutant, or human wild-type STAT5B or the hyperactive N642H STAT5B mutant (STAT5BN642H). In graphs, each symbol represents a mouse, and lines represent the median. $^{**}P < 0.01$, $^{***}P < 0.001$, $^{****}P < 0.0001$ using ordinary 1-way ANOVA with Tukey's multiple-comparisons test. (**A**) Expression of CD27 and CD44 in order to identify CD27⁻CD44⁺ γδT17 cells in the LN. Numbers indicate percentage of CD27⁻CD44⁺ or CD27⁺ within the γδ T cell compartment. (**B**) Numbers of γδT17 (staining as in **A**) and CD27⁺ cells in the LN. (**C**) Expression of IL-17A within the LN γδ T cell compartment (single asterisk in STAT5BN642H denotes difference by comparison with STAT5AS710F^{low}). (**D**) Expression of CCR6 and Vγ4 in skin γδT17 cells (staining as in Figure 1B). Numbers indicate percentage of CCR6⁺ or CCR6⁻ cells within the γδ T cell compartment. (**E**) Numbers of CCR6⁺ and CCR6⁻ cells identified in **D**. (**F**) Ratio of CCR6⁺ over CCR6⁻ cells in WT compared with STAT5AS710F^{high} (5A) and STAT5BN642H (5B) mice. (**A**–**E**) n = 8 WT, 8 STAT5AS710F^{low}, 8 STAT5AS710F^{high}, 7 STAT5B, and 5 STAT5BN642H mice, 2 experiments.

in STAT5 equally affected both Vγ4⁺ and Vγ4⁻ subsets of γδT17 cells (not shown) (Vγ nomenclature according to Heilig and Tonegawa) (40). Interestingly, RORγt^{CRE}-STAT5$^{F/F}$ mice had a concomitant increase in IFN-γ–expressing and CD27⁺ γδ T cells (Figure 1C). In RORγt^{CRE}-STAT5$^{F/F}$ mice, deletion of STAT5 in CD4⁺ and CD8⁺ T cells was not complete (Supplemental Figure 1A; supplemental material available online with this article; https://doi.org/10.1172/JCI131241DS1). Insufficient deletion in the αβ T cell compartment using RORγt^{CRE} deleter mice is explained by the low activity of the Cre recombinase in these subsets (41). Consequently, we did not observe differences in the numbers of TCRβ⁺CD4⁺CCR6⁺ cells, which are enriched for Th17 cells (Supplemental Figure 1B), or in the frequency of IFN-γ–producing CD4⁺ T cells (Supplemental Figure 1B). Surprisingly, and also in agreement with previous observations (42), the percentage of IL-17A–producing CD4⁺ T cells was higher even when STAT5 was only partially deleted (Supplemental Figure 1B). To test whether lack of STAT5 affected other RORγt-expressing innate T cell populations, we enumerated IL-17A⁺TCRγδ⁻ cells in the LNs of RORγt^{CRE}-STAT5$^{F/F}$ mice and found a significant reduction in their numbers compared with those in controls (Supplemental Figure 1C), indicating that STAT5 may be important for more than one innate T cell subset.

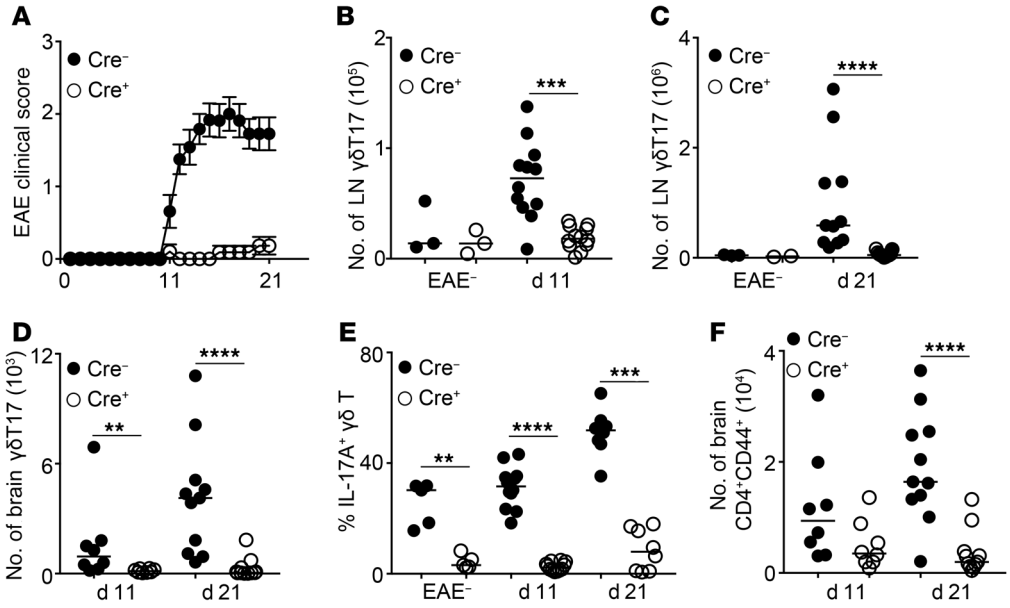

Figure 3. RORγt^{CRE}-STAT5$^{F/F}$ mice are resistant to EAE. Disease progression and flow cytometric analysis of γδ and CD4$^+$ T cells in RORγt^{CRE}-STAT5$^{F/F}$ (Cre$^+$) and littermate control mice (Cre$^-$) that had been previously immunized with 50 μg MOG peptide in CFA and 200 ng pertussis toxin. In graphs, each symbol represents a mouse, and lines represent the median (except in **A**). $^{**}P < 0.01$, $^{***}P < 0.001$, $^{****}P < 0.0001$ using Mann-Whitney test. (**A**) Clinical symptoms of EAE until day 21 after immunization. Data are pool of 20 mice per genotype and shown as mean ± SEM. Statistical analysis was performed using 2-way ANOVA with Bonferroni's multiple-comparisons test. ANOVA $P < 0.0001$; Bonferroni's test returned significance for days 11–21 with day 11 $P = 0.003$ and days 12–21 $P < 0.0001$. (**B** and **C**) Numbers of γδT17 cells in the LN (staining as in Figure 1A) of unimmunized controls (EAE$^-$) and at 11 (**B**) and 21 (**C**) days after immunization. (**D**) Numbers of γδT17 cells in the brain (identified as CD45$^+$CD3$^+$TCRβ$^-$TCRγδ$^+$CD44$^+$CD27$^-$) at days 11 and 21 after immunization. (**E**) Expression of IL-17A within the LN γδ T cell compartment of unimmunized controls (EAE$^-$) and at 11 and 21 days after immunization. (**F**) Numbers of CD4$^+$CD44$^+$CD3$^+$TCRβ$^+$ cells in the brain at days 11 and 21 after immunization. (**B**, **C**, and **E**) n = 11–12 mice (d11/21) and 2–8 mice (EAE$^-$), 3 experiments; (**D** and **F**) n = 4–6 mice (EAE$^-$), 8 mice (d11), and 11 mice (d21), 3 experiments.

In order to determine whether the defect we observed in RORγt^{CRE}-STAT5$^{F/F}$ mice was intrinsic to the γδT17 population, we generated mixed bone marrow chimeras using CD45.1$^+$ WT and Cre$^+$ CD45.2$^+$ donors and analyzed LNs and skin 12 weeks later. We found that by comparison with WT, RORγt^{CRE}-STAT5$^{F/F}$ bone marrow failed to generate γδT17 cells, suggesting that the STAT5-associated defect is cell-intrinsic (Supplemental Figure 2A). It is noteworthy that in the skin we could not detect any γδT17 cells originating from RORγt^{CRE}-STAT5$^{F/F}$ bone marrow (Supplemental Figure 2A). Because γδT17 cells are embryonic and neonatal in nature, we reasoned that an adult stem cell niche in the bone marrow might misrepresent the requirements of thymically exported cells after birth. We therefore isolated γδ T cells from neonatal thymi of RORγt^{CRE}-STAT5$^{F/F}$ and littermate control mice, mixed them 1:1, and transferred them to recombinase-activating gene-1–deficient (*Rag1*$^{-/-}$) hosts. We found that STAT5-sufficient cells outcompeted their STAT5-deficient counterparts, suggesting that STAT5 is required cell-intrinsically for maintaining γδT17 cells (Supplemental Figure 2B).

We next investigated whether reduced γδT17 cell numbers in the absence of STAT5 were due to a developmental defect. We examined newborn thymi from RORγt^{CRE}-STAT5$^{F/F}$ and littermate control mice and found no differences in γδT17 cellularity (Figure 1D) or IL-17A expression (Supplemental Figure 3A). Expression of both *Stat5a* and *Stat5b* was significantly lower in RORγt^{CRE}-STAT5$^{F/F}$ γδT17 cells sorted from newborn thymi compared with Cre$^-$ controls or CD27$^+$ γδ T cells (Supplemental Figure 3B). Separating the newborn γδT17 population into Vγ4$^+$ and Vγ4$^-$ cells did not show any subset-specific differences (Supplemental Figure 3C). Since the Vγ4$^-$ population is heterogeneous and may be composed of cells expressing Vγ6, Vγ1, and Vγ2, we stained for these TCRγ chains and found no significant differences in the numbers of γδT17 cells between STAT5-deficient and STAT5-sufficient cells in the newborn thymus (Supplemental Figure 3D). We additionally analyzed Vγ4$^+$ and Vγ6$^+$ cells in embryonic day 16 thymi of RORγt^{CRE}-STAT5$^{F/F}$ and littermate control mice. At that developmental stage Vγ4- and Vγ6-expressing cells were either CD27$^+$ or CD27$^-$; however, lack of STAT5 did not impact on their numbers (Supplemental Figure 3E). This suggested that the major impact of STAT5 occurs extrathymically. We thus analyzed neonatal mice and found a significant decrease in LN γδT17 cell numbers in 7- and 14-day-old mice (Figure 1E). Assessment of proliferation by Ki67 staining showed that γδT17 cells in RORγt^{CRE}-STAT5$^{F/F}$ neonatal mice displayed reduced turnover compared with controls (Figure 1F). Furthermore, expression of the antiapoptotic STAT5 target gene product BCL2 (23, 43) was reduced in neonatal STAT5-deficient γδT17 cells (Supplemental Figure 3F), suggesting impaired survival. Collectively, we demonstrate that STAT5 is important for the turnover and survival of γδT17 cells during neonatal and adult life.

Differential regulation of γδT17 and CD27$^+$ γδ T cells by STAT5A and STAT5B. Since deficiency in STAT5 resulted in near-complete loss of γδT17 cells, we next examined the influence of hyperactive STAT5 expression. We used 2 established models of STAT5

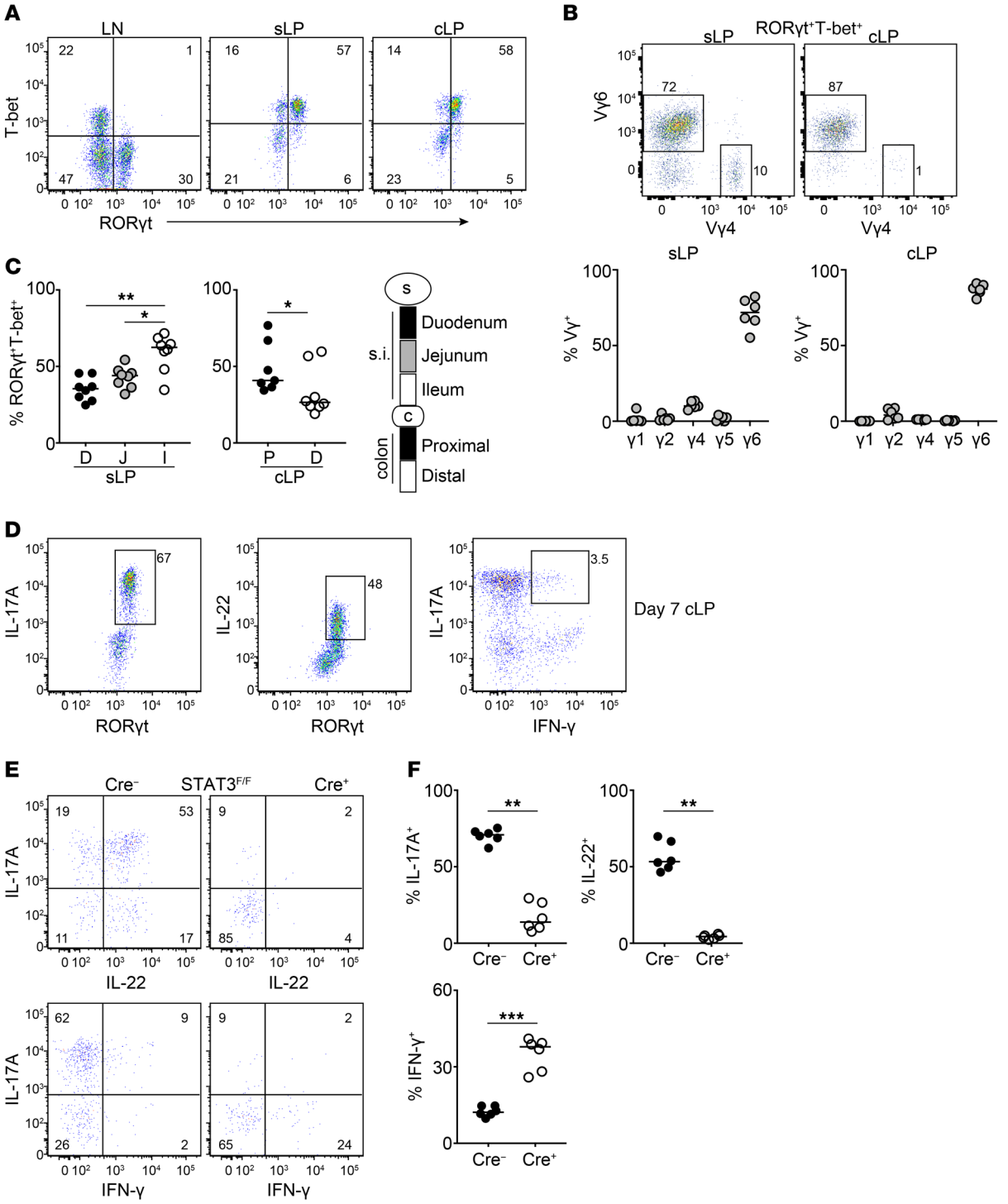

Figure 4. Intestinal γδT17 cells express T-bet and require STAT3 for IL-17A and IL-22. Flow cytometric analysis of LN and intestinal γδ T cells in WT (C57BL/6), RORγt^{GFP}T-bet^{AmCyan}, or in RORγt^{CRE}-STAT3$^{F/F}$ (Cre$^+$) and littermate control mice (Cre$^-$). In graphs, each symbol represents a mouse, and lines represent the median. Cytokine detection was performed following IL-23 restimulation. $^*P < 0.05$, $^{**}P < 0.01$, $^{***}P < 0.001$ using Mann-Whitney test. (**A**) Expression of RORγt and T-bet within the γδ T cell compartment of the LN, sLP, and cLP. Numbers indicate percentage of RORγt and T-bet expression. (**B**) Expression of Vγ6 and Vγ4 and frequency of Vγ1-, Vγ2-, Vγ-4, Vγ5-, and Vγ6-expressing RORγt$^+$T-bet$^+$ γδ T cells in the cLP and sLP (using RORγt^{GFP}T-bet^{AmCyan} double-reporter mice). (**C**) Frequency of RORγt$^+$T-bet$^+$ cells within the γδ T cell compartment in the indicated small intestinal (s.i.) and colonic segments. (**D**) Expression of RORγt and IL-17A, RORγt and IL-22, or IL-17A and IFN-γ in the γδ T cell compartment of cLP from 7-day-old mice (representative of 2 experiments). (**E**) Expression of IL-17A and IL-22 (top) or IL-17A and IFN-γ (bottom) in the cLP of RORγt^{CRE}-STAT3$^{F/F}$ (Cre$^+$) and littermate control mice (Cre$^-$). Numbers indicate percentage of positive expression. (**F**) Frequency of IL-17A$^+$, IL-22$^+$, and IFN-γ$^+$ γδ T cells in the cLP of RORγt^{CRE}-STAT3$^{F/F}$ (Cre$^+$) and littermate control mice (Cre$^-$). (**A**) n = 10–14 mice, 6 experiments; (**B**) n = 6 mice, 2 experiments; (**C**) n = 8 mice, 4 experiments; (**D**) n = 8 mice, 2 experiments; (**E** and **F**) n = 6 mice, 2 experiments.

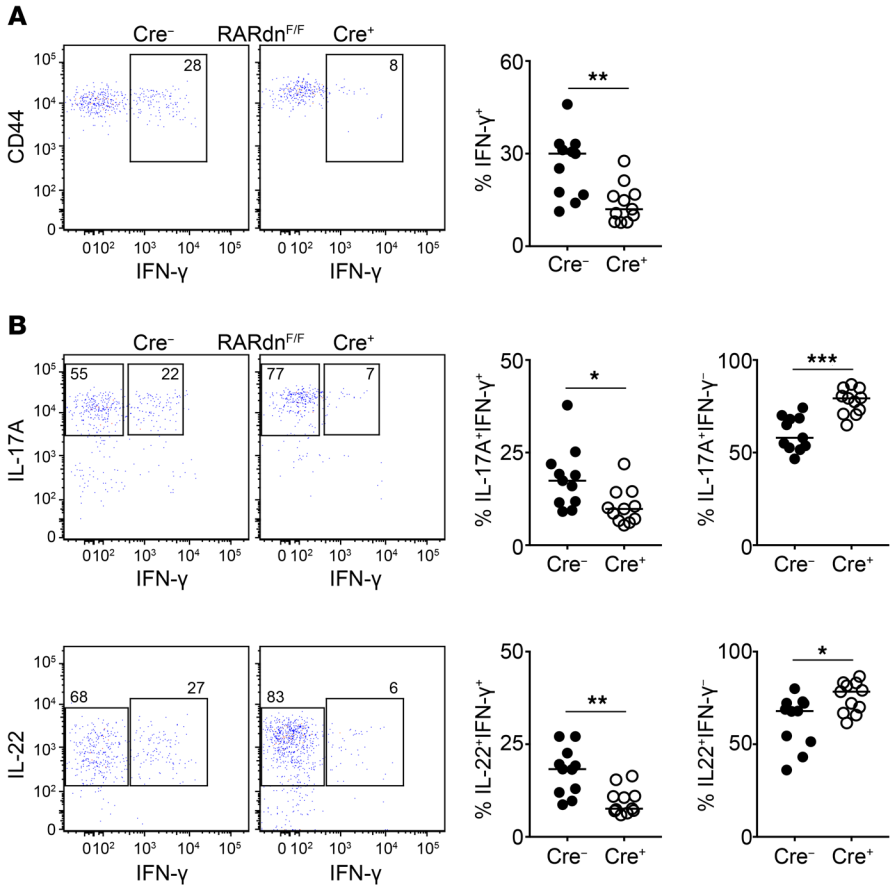

Figure 5. Retinoic acid receptor signaling regulates IFN-γ production in intestinal T-bet⁺ γδT17 cells. Flow cytometric analysis of cytokine expression in colonic γδ T cells in RORγt^{CRE}-RARdn$^{F/F}$ (Cre⁺) and littermate control mice (Cre⁻) following IL-23 stimulation. In graphs, each symbol represents a mouse, and lines represent the median. $*P < 0.05$, $**P < 0.01$, $***P < 0.001$ using Mann-Whitney test. (**A**) Expression of CD44 and IFN-γ (dot plots) and frequency of IFN-γ⁺ γδ T cells (graph) in RORγt^{CRE}-RARdn$^{F/F}$ (Cre⁺) and littermate control mice (Cre⁻). (**B**) Expression of IL-17A and IFN-γ (top dot plots) or IL-22 and IFN-γ (bottom dot plots) with graphical representation of the frequency of IL-17A⁺IFN-γ⁺ and IL-17A⁺IFN-γ⁻ or IL-22⁺IFN-γ⁺ and IL-22⁺IFN-γ⁻ γδ T cells in RORγt^{CRE}-RARdn$^{F/F}$ (Cre⁺) and littermate control mice (Cre⁻). (**A** and **B**) $n = 11$ mice, 5 experiments.

hyperactivity whereby the *Vav1* promoter drives the expression of (a) high or low copies of the hyperactive S710F *STAT5A* mutant (44, 45), or (b) human WT or the hyperactive N642H *STAT5B* mutant (30). Constitutively high levels of hyperactive STAT5A resulted in very high numbers of γδT17 cells in LNs, but hyperactivation of STAT5A had a considerably smaller impact on CD27⁺ γδ T cells (Figure 2, A and B). In contrast, constitutive expression of hyperactive STAT5B increased the numbers of CD27⁺ γδ T but had a smaller effect on γδT17 cells (Figure 2, A and B). When we analyzed cytokine expression, we found that IFN-γ was only induced by hyperactive STAT5B (Supplemental Figure 4A), whereas IL-17A could be induced at high levels by both hyperactive STAT5A and WT STAT5B expression (Figure 2C). However, hyperactive STAT5B did not induce IL-17A expression (Figure 2C). In order to test whether the differences we detected were due to varying activity levels between the 2 hyperactive transgenes, we purified CD27⁺ and γδT17 cells from the LNs of STAT5AS710F^{high} and STAT5B^{N642H} mice and analyzed expression of some of the common STAT5A/B target genes (44) as a surrogate for transgene activity. We found that none of the STAT5A/B target genes were differentially regulated within the 2 populations (Supplemental Figure 4B), suggesting that there is no difference in the activity level of the transgenes.

Skin γδT17 cell numbers, like those in the LN, were greatly enhanced by hyperactive STAT5A, whereas STAT5B had a milder impact (Figure 2, D and E). With the exception of Vγ5⁺ dendritic epidermal T cells, CCR6⁺ γδT17 cells are the only γδ population in the skin. However, mice expressing hyperactive STAT5B, and to a lesser extent mice expressing hyperactive STAT5A, contained CCR6⁻ γδ T cells that were either Vγ4⁺ or Vγ4⁻ (Figure 2, D–F). Collectively, our data point toward a dominant role of STAT5A in supporting γδT17 cells in LN and skin, with STAT5B supporting mainly IFN-γ–producing and CCR6⁻ γδ T cells.

RORγt^{CRE}-STAT5$^{F/F}$ mice are resistant to EAE. γδT17 cells have been implicated in the pathogenesis of EAE (3, 46), and we therefore investigated how well RORγt^{CRE}-STAT5$^{F/F}$ mice responded to myelin oligodendrocyte glycoprotein–induced (MOG-induced) EAE. We found that compared with littermate controls, RORγt^{CRE}-STAT5$^{F/F}$ mice were resistant to EAE symptoms (Figure 3A). This correlated with significantly reduced γδT17 cells in the LN and brain at days 11 and 21 after immunization (Figure 3, B–D). As expected, γδ T cell–associated IL-17A production was significantly reduced at all time points in mice lacking STAT5 (Figure 3E). Although it has been recently suggested that inflammatory conditions during EAE can regenerate γδT17 cells de novo (47), our data suggest that in the absence of STAT5, γδT17 cell regeneration cannot occur.

It has been shown that in addition to their direct contribution to EAE pathogenesis, γδT17 cells are required for optimal Th17 responses (3). We therefore interrogated the CD4⁺ T cell response in the LN and brain of RORγt^{CRE}-STAT5$^{F/F}$ and littermate control mice during EAE. We found that the numbers and cytokine production of CD4⁺ T cells were not affected in the LN (Supplemental Figure 1, D and E), which may reflect the levels of STAT5 still

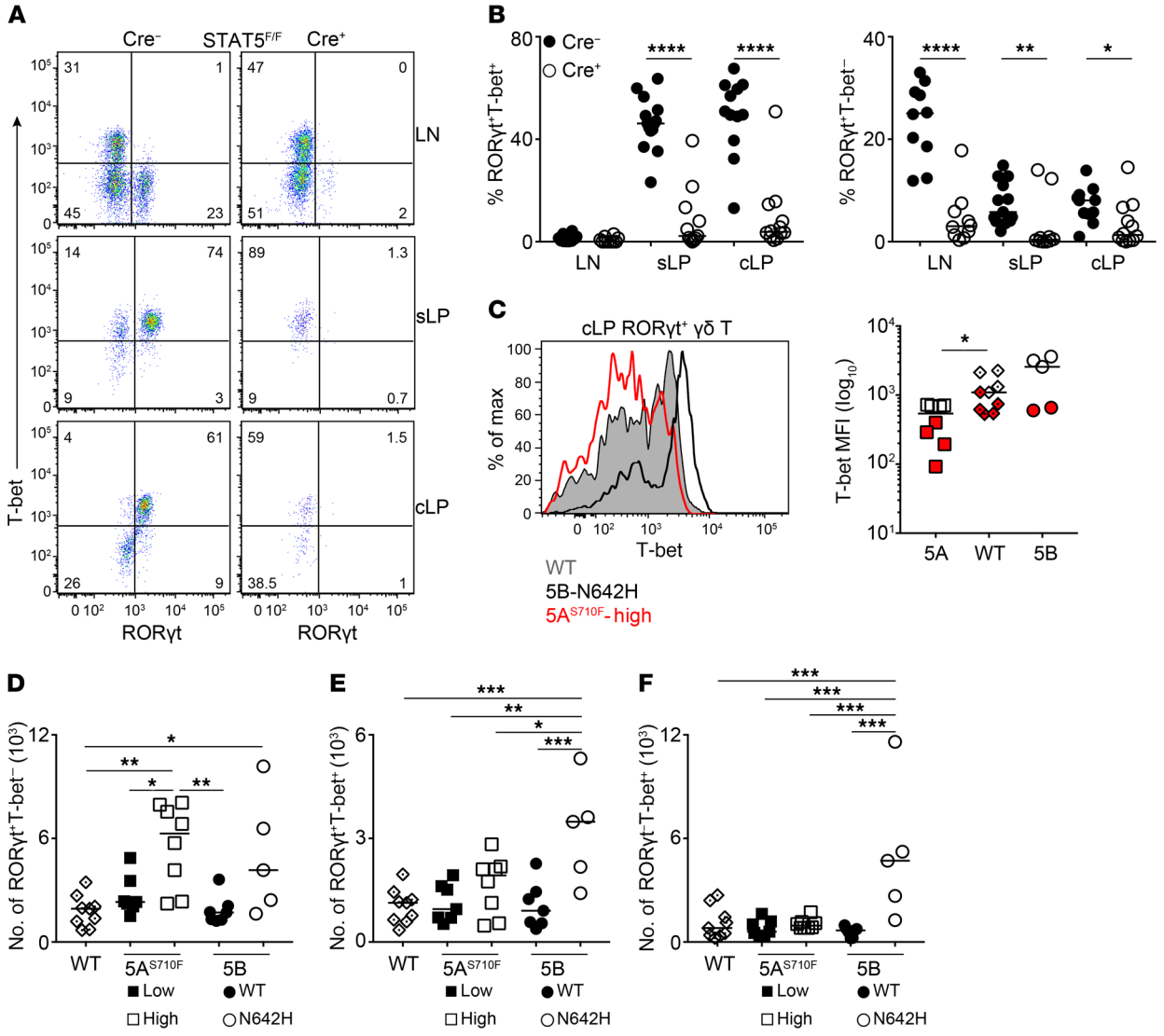

Figure 6. STAT5 is a critical determinant of T-bet–expressing intestinal γδT17 cells. Flow cytometric analysis of intestinal γδ T cells in RORγt^{CRE}-STAT5$^{F/F}$ (Cre$^+$) and littermate control mice (Cre$^-$) or in hyperactive STAT5A and STAT5B mutant mice as described in Figure 2. In graphs, each symbol represents a mouse, and lines represent the median. *P < 0.05, **P < 0.01, ***P < 0.001, ****P < 0.0001 using Mann-Whitney test (**A**–**C**) or ordinary 1-way ANOVA with Tukey's multiple-comparisons test (**D**–**F**). (**A**) Expression of RORγt and T-bet within the γδ T cell compartment of the LN, sLP, and cLP. Numbers indicate percentage of RORγt and T-bet expression. (**B**) Frequency of RORγt$^+$T-bet$^+$ and RORγt$^+$T-bet$^-$ cells within the γδ T cell compartment in LN, sLP, and cLP. (**C**) Expression of T-bet (histogram) and T-bet mean fluorescence intensity (MFI) (graph) in RORγt$^+$ cLP γδ T cells from WT, STAT5AS710F^{high} (5A), or STAT5B-N642H (5B) mice as described in Figure 2. In the graph, colors indicate 2 different experiments. (**D**–**F**) Numbers of RORγt$^+$T-bet$^-$ (**D**), RORγt$^+$T-bet$^+$ (**E**), and RORγt$^-$T-bet$^+$ (**F**) γδ T cells in the cLP of the indicated hyperactive STAT5A and STAT5B mutant mice or WT control mice. (**A** and **B**) n = 10–14 mice, 6 experiments; (**C**–**F**) n = 8 WT, 8 STAT5AS710F^{low}, 8 STAT5AS710F^{high}, 7 STAT5B, and 5 STAT5BN642H mice, 2 experiments.

detectable in these cells (Supplemental Figure 1A). As expected from the clinical score and the lack of proinflammatory γδT17 cells, there was a profound reduction in CD4$^+$ T cell numbers within the brain of RORγt^{CRE}-STAT5$^{F/F}$ mice (Figure 3F). Collectively, our data show that loss of γδT17 cells due to STAT5 deficiency is associated with dramatically reduced inflammatory responses in the EAE model.

Intestinal lamina propria γδT17 cells express T-bet and require STAT3 and retinoic acid for cytokine production. Besides the skin and peripheral lymphoid tissues, γδ T cells with type 3 functionality have been described in the mucosa, such as the lung and gut (48, 49). We therefore wanted to test whether STAT5 regulated γδT17 cells specifically in the intestinal lamina propria. In order to avoid potential differences in γδT17 surface markers in the gut, we stained small intestinal and colonic lamina propria (sLP and cLP, respectively) for RORγt and T-bet and compared this with peripheral LNs. Surprisingly, we found that many RORγt$^+$ γδ T cells in the gut coexpressed T-bet (Figure 4A). We additionally confirmed the presence of RORγt$^+$T-bet$^+$ γδ T cells by generating double-transgenic mice reporting GFP and AmCyan under control of the promoters for *Rorc* and *Tbx21*, respectively (Supplemental Figure 5A). Of the RORγt$^+$T-bet$^+$ γδ T cells, approximately 70%–80% in the sLP and 90% in the cLP were Vγ6$^+$, the remaining cells being mostly Vγ4$^+$ (Figure 4B). By transcription factor

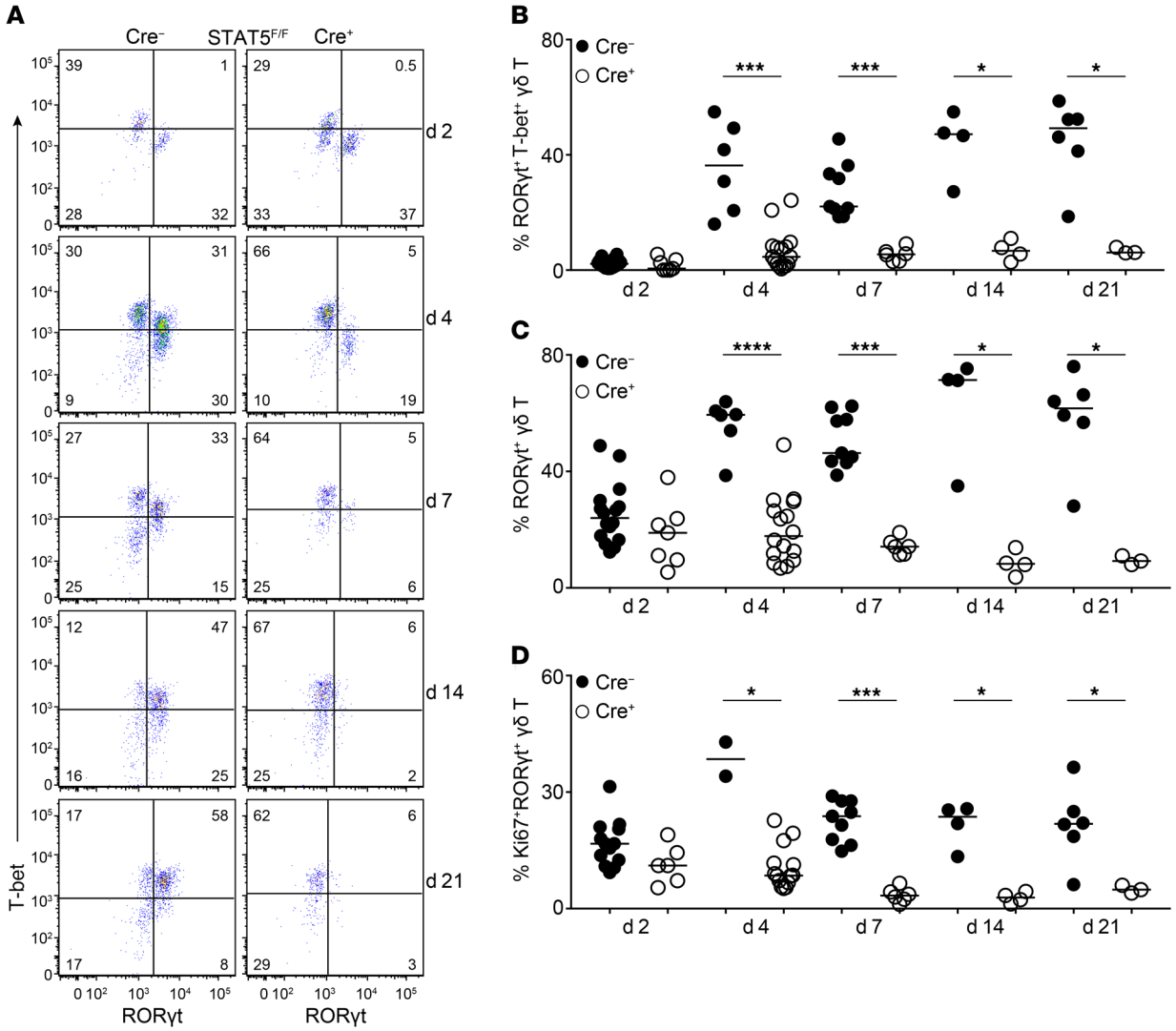

Figure 7. STAT5 regulates the neonatal fate of intestinal T-bet⁺ γδT17 cells. Flow cytometric analysis of colonic γδ T cells in RORγt^{CRE}-STAT5$^{F/F}$ (Cre⁺) and littermate control mice (Cre⁻) during neonatal ontogeny. Day of birth is counted as day 1 (d1). In graphs, each symbol represents a mouse, and lines represent the median. *P < 0.05, ***P < 0.001, ****P < 0.0001 using Mann-Whitney test. (**A**) Expression of RORγt and T-bet within the γδ T cell compartment of cLP at the indicated days after birth. Numbers indicate percentage of RORγt and T-bet expression. (**B**) Frequency of cLP RORγt⁺T-bet⁺ γδ T cells at the indicated days after birth. (**C**) Frequency of cLP RORγt⁺ γδ T cells (including T-bet⁺) at the indicated days after birth. (**D**) Frequency of cLP Ki67⁺RORγt⁺ γδ T cells at the indicated days after birth. (**A**–**D**) n = 2–16 mice from at least 5 different litters.

staining analysis, we found that the RORγt⁺T-bet⁺ γδ T cell population was more prevalent in the ileum and proximal colon (Figure 4C), which contrasted with the distribution of RORγt⁻T-bet⁺ γδ T cells in the same locations (Supplemental Figure 5B). In order to investigate which factors regulate the expression of T-bet, we analyzed mice deficient in Toll-like receptor and IL-12 signaling as well as mice depleted of their intestinal microbial flora. We found that expression of T-bet was independent of the microbiota (Supplemental Figure 5C), MyD88, TRIF, and IL-12 signaling (Supplemental Figure 5D).

In agreement with their innate nature, intestinal γδT17 cells produced IL-17A, IL-22, and IFN-γ as early as 7 days after birth (Figure 4D), indicating a functional γδT17 population that has acquired the ability to produce IFN-γ at steady state. Using RORγt^{CRE}-STAT3$^{F/F}$ mice, we recently showed that STAT3 is critical for the production of IL-17A/F and IL-22 by activated γδT17 cells (41). Similarly, we found that in intestinal γδT17 cells production of both IL-17A and IL-22 was STAT3-dependent (Figure 4, E and F, and Supplemental Figure 6, A and B). One of the key factors regulating IFN-γ–expressing cells is retinoic acid (RA) (50). We therefore examined mice possessing an RA receptor–dominant-negative (RARdn) transgene, which prevents active RARα signaling (51) in RORγt-expressing cells (RORγt^{CRE}-RARdn$^{F/F}$ mice). We found that loss of RA signaling was associated with reduced overall expression of IFN-γ (Figure 5A and Supplemental Figure 6C) as well as reduced frequency of IL-17A⁺IFN-γ⁺ and IL-22⁺IFN-γ⁺ cells (Figure 5B and Supplemental Figure 6D). In contrast, deficiency in RA signaling resulted in significantly increased frequency of IL-17A⁺IFN-γ⁻ and IL-22⁺IFN-γ⁻ T-bet⁺ γδT17 cells in the colon and small intestine (Figure 5B and Supplemental Figure 6D). Collectively, these data indicate that lamina propria T-bet⁺ γδT17 cells are innate cells that can coproduce

IL-17, IL-22, and IFN-γ, and that their cytokine expression profile is regulated by STAT3 and RA.

STAT5 regulates T-bet expression and determines the progression of intestinal γδT17 cells through neonatal development. Following the identification of a distinct gut-specific γδT17 population, we aimed to understand its dependence on STAT5. Like those from LNs, RORγt-expressing γδ T cells, irrespective of T-bet, were drastically and significantly reduced from the sLP and cLP of RORγt^{CRE}-STAT5$^{F/F}$ mice (Figure 6, A and B). Analysis of GOF *STAT5A* and *STAT5B* mice revealed that hyperactive STAT5A downregulated T-bet in RORγt$^+$ cLP γδ T cells, whereas hyperactive STAT5B enhanced it (Figure 6C), suggesting a yin/yang regulation in RORγt$^+$ cLP γδ T cells by STAT5A versus STAT5B. Hyperactive STAT5A preferentially expanded RORγt$^+$ cells in the gut, whereas hyperactive STAT5B favored T-bet–expressing γδ T cells irrespective of whether they expressed RORγt (Figure 6, D–F).

Next, we sought to determine whether STAT5 also regulated RORγt$^+$T-bet$^+$ γδ T cells neonatally. We therefore analyzed neonatal gut at different time points and found that 1–2 days after birth γδ T cells in the colon and small intestine expressed either RORγt or T-bet but not both (Figure 7, A–C, and Supplemental Figure 7, A–C). T-bet was induced in RORγt-expressing cells at day 4 and stabilized to adult levels within the first week of life (Figure 7, A and B, and Supplemental Figure 7, A and B). Expression of T-bet at neonatal day 4 coincided with a rapid increase in cell proliferation, which was blunted in the absence of STAT5 (Figure 7D and Supplemental Figure 7D). RORγt^{CRE}-STAT5$^{F/F}$ mice did not upregulate T-bet and failed to sustain a RORγt$^+$ γδ T cell population after birth (Figure 7, A–C, and Supplemental Figure 7, A–C). However, despite their functional presence in the neonatal gut, RORγt-expressing γδ T cells were not necessary for protection against early-life infection with the attaching and effacing bacterium *Citrobacter rodentium* (Supplemental Figure 8, A–C).

Collectively, our data demonstrate that during neonatal life STAT5 acts as a molecular checkpoint to promote proliferation of intestinal γδT17 cells. Moreover, our data reveal an interesting balance between STAT5A and STAT5B, which appear to have opposing roles in the regulation of T-bet expression, thereby differentially coordinating tissue specificity of γδT17 cells.

Discussion

In the present study we demonstrate that STAT5 is a critical regulator of IL-17–producing γδ T cells in the periphery, skin, and gut. STAT5 was necessary during neonatal life in order to sustain proliferation and survival of γδT17 cells. Transgenic reconstitution of hyperactive STAT5 variants showed that STAT5A preferentially sustains γδT17 whereas STAT5B promotes IFN-γ–producing γδ T cells. Physiologically, hampered development of γδT17 cells due to STAT5 loss resulted in resistance to EAE pathology and prevented Th17 cells from infiltrating the brain. Furthermore, we discovered that intestinal lamina propria γδT17 cells coexpress the type 1 transcription factor T-bet and can produce IL-17, IL-22, and IFN-γ in a STAT3- and RA-dependent mechanism. Intestinal γδT17 cells upregulate T-bet during the first week of life and are strictly STAT5-dependent for their neonatal development. Furthermore, expression of T-bet is under the antagonistic control of STAT5A and STAT5B.

STAT5 is a major signaling component downstream of many cytokine and growth factor receptors and is therefore involved in the development of lymphocyte lineages (52). Hence, both mice and humans with STAT5-associated deficiencies are severely immunocompromised (24, 53). T cells of the γδ lineage are reduced in the thymus and lymphoid tissues of fully STAT5-deficient mice (21), and this has been attributed to a failure to successfully rearrange the TCR early during embryonic development (26). However, our data show that γδT17 cells require STAT5 signaling to expand and survive after they exit the thymus. This suggests that γδ T cell subsets rely on STAT5 during different steps of their development and differentiation, presumably reflecting cytokine niches within the local microenvironment.

Detailed molecular and phenotypic studies using mice deficient in either STAT5A or STAT5B have shown that despite their many commonalities, particularly at the genome-wide level, the 2 STAT5 gene products can display cell-specific functions (19, 25). Thus, in CD4$^+$ T cells STAT5B has a dominant role in orchestrating differentiation and function. In this regard, our data show that both STAT5A and STAT5B can have dominant and differential roles in γδ T cells depending on the specific subset. Whereas STAT5A regulated almost exclusively γδT17 cells and downregulated intestinal T-bet expression, STAT5B had a prevailing effect on IFN-γ–expressing γδ populations. This suggests that, unlike in CD4$^+$ helper and innate lymphoid cells, STAT5A and STAT5B display significant, differential regulatory functions in γδ T cell subsets, and further points to the distinct molecular, functional, and developmental requirements of γδT17 compared with non–IL-17–producing subsets. The unique roles that we uncovered herein for STAT5A and STAT5B suggest that they display cell-specific functions and can have context-dependent, nonredundant roles in generating robust immune responses. The genetic and cellular tools that we used herein will be crucial to illuminate the specific biological functions of these 2 highly species-conserved proteins that play indispensable roles in infection, cancer, and autoimmunity.

Although γδT17 cells develop in the embryonic thymus, previous reports suggested that they populate the skin and LNs after birth (17). Findings herein indicate that the neonatal period is critical for γδT17 cells to populate lymphoid and nonlymphoid tissues. A critical time window of opportunity has been suggested to exist in neonatal life during which exposure to the microbiota matures the immune system to acquire productive cellular and humoral immunity (54, 55). The upregulation of T-bet in murine intestinal γδT17 cells within days after birth and its independence of the microbiota and TLR signals suggest alternative neonatal factors such as lactation, which is predominantly STAT5A-controlled (56). Neonatal-specific cytokine milieus that activate STAT5 may also regulate T-bet expression in the developing gut. In this regard, hyperactive STAT5A downregulated T-bet whereas high STAT5B activity induced it, although whether this was direct or indirect through regulation of cell fate transcriptional regulators remains to be studied. Nevertheless, the identification of T-bet–expressing γδT17 cells at steady state indicates a form of plasticity within this lineage that is regulated post-thymically and in a tissue-specific manner. The importance of T-bet in γδT17 cells is currently unknown. However, the coexpression of IFN-γ suggests that acquisition of type 1 transcriptional and functional traits may give

an advantage over infection, similar to innate lymphoid cells and Th1-transitioning Th17 cells.

Animal models have linked γδT17 cells to immune responses during inflammation, infection, and cancer where they can be either protective or pathogenic (57). In the imiquimod model of psoriasis, γδT17 cells are important to drive disease; however, when absent, their pathogenic role can be compensated by other inflammatory cells (58). In the EAE mouse model, γδT17 cells have also been shown to contribute to pathogenicity (3, 46). Herein, we provide evidence that γδT17 cells are important for the development of EAE symptoms and for the mobilization of Th17 cells to the brain. Despite their absence from all major organs from neonatal life onward, other innate inflammatory cells could not compensate. γδ T cells have coevolved alongside αβ T and B cells (59); however, their function has diversified and was imprinted by the specific tissue cues present in different locations. It is thus not surprising that the immunological response of different γδ T cell subsets will vary and will be essential or redundant depending on the inflammatory or infectious context.

The JAK/STAT pathway has been a therapeutic target for many years, and successful small-molecule inhibitors have been approved or are in clinical trials for the treatment of inflammatory diseases (e.g., rheumatoid arthritis) and cancer (e.g., leukemia) (60, 61). Increasing evidence points toward the importance of γδ T cells as pathogenic in inflammation (57), as pro- or antitumorigenic mediators (62), whereas their neoplastic transformation can lead to rare but aggressive lymphomas (35). Our findings are in line with the notion that targeting of the JAK/STAT pathway, particularly STAT5, may have significant clinical implications in cancer and inflammation through interfering with basic γδ T cell development, activation, and tissue plasticity.

Methods

Mice. RORγt^{CRE} and RORγt^{GFP} mice (63) were provided by Gerard Eberl (Pasteur Institute, Paris, France) and subsequently bred in-house. STAT5$^{F/F}$ mice were generated as previously described (39) and bred in-house. STAT3$^{F/F}$ mice were purchased from The Jackson Laboratory (stock 028526) and bred in-house. RARdn$^{F/F}$ mice, generated as previously described (51), were provided by William W. Agace (Lund University, Lund, Sweden) and bred in-house. Intestinal tissue from *Il12*$^{-/-}$ mice (stock 002692) and *Rag1*-deficient mice was provided by William W. Agace. GOF *STAT5A* and *STAT5B* mice were generated as previously described (30, 44) and were bred at the University of Veterinary Medicine Vienna. Frozen sperm samples from *Tbx21*-AmCyan mice (64) were provided by Jinfang Zhu (National Institute of Allergy and Infectious Diseases, NIH, Rockville, Maryland, USA), and after re-derivation, mice were bred in-house. Intestinal tissue from mice deficient in TRIF and MyD88 was provided by Katharina Lahl (Technical University of Denmark). WT C57BL/6 mice were purchased from Taconic and bred in-house.

Cell culture media and buffers. All cell culture and single-cell suspensions were prepared using RPMI 1640 (Invitrogen) supplemented with 10% heat-inactivated FBS (Thermo Fisher Scientific), 20 mM HEPES (pH 7.4; Thermo Fisher Scientific), 50 μM 2-mercaptoethanol, 2 mM L-glutamine (Thermo Fisher Scientific), and 10,000 U/mL penicillin-streptomycin (Thermo Fisher Scientific). 10× HBSS (Thermo Fisher Scientific) was diluted to 1× with sterile nuclease-free water and supplemented with 15 mM HEPES (pH 7.4; Thermo Fisher Scientific) to prepare HBSS-HEPES, or supplemented with 2 mM EDTA, 15 mM HEPES, 50 μg/mL gentamycin, and 2% FBS to prepare HBSS-EDTA. Isotonic Percoll was prepared by mixing of 90% vol/vol of Percoll (GE Healthcare) with 9% vol/vol 10× HBSS and 1% vol/vol 1-M HEPES (pH 7.4). Isotonic Percoll was subsequently diluted with HBSS-EDTA to the desired concentration. FACS buffer was prepared by mixing of 3% heat-inactivated FBS with DPBS (Thermo Fisher Scientific). MACS buffer was prepared by mixing of 2% heat-inactivated FBS and 1 mM EDTA with DPBS.

Isolation of lymphocytes from LNs, thymus, skin, small intestine, and colon. LNs were dissected, cleared of fat, and crushed against a 70-μm cell strainer to prepare single-cell suspensions. Cell suspensions were then washed and filtered through a 40-μm cell strainer. Cells were counted, and 2.5×10^6 cells were used for staining of surface antigens and flow cytometry analysis. Thymus lobes from embryonic day 16 fetuses and 2-day-old (1 day after birth) pups were dissected and dissociated in supplemented RPMI using a dissection microscope to prepare single-cell suspension. The cell suspensions were filtered through a 40-μm cell strainer and stained for surface antigens under sterile conditions before FACS sorting.

Skin lymphocytes were prepared from ears as follows: first, the dorsal and ventral sides of the ears were mechanically separated; they were subsequently cut into small pieces, followed by enzymatic digestion with 0.25 mg/mL collagenase IV, 0.166 mg/mL hyaluronidase, and 0.1 mg/mL DNase I (all enzymes from Sigma-Aldrich) in supplemented RPMI for 1 hour at 37°C with constant stirring at 700 rpm. Undigested tissue was crushed against a 70-μm cell strainer to prepare a single-cell suspension. After washing, the cell pellet was resuspended and filtered through a 40-μm cell strainer to remove tissue debris and used for flow cytometry staining.

Small intestines and colons were dissected from adult mice and were flushed with 20 mL HBSS-HEPES to remove intestinal contents. Fat and Peyer's patches were removed, and then the tissues were opened longitudinally and cut into small pieces of approximately 2–3 cm. Chopped tissue was washed 4 times (2 alternate cycles of 10 and 15 minutes each) using 15 mL of HBSS-EDTA buffer at 37°C in a shaking incubator. Tissue pieces were then digested using 0.3 mg Liberase TM (Roche) and 0.15 mg of DNase (Sigma-Aldrich) per preparation in 5 mL supplemented RPMI for 40 minutes on the magnetic stirrer at 37°C. The resulting cell suspensions were filtered through 70-μm cell strainers, collected in complete RPMI, and subsequently pelleted by centrifugation. The cell pellets were then resuspended in 5 mL 40% Percoll, layered on 4 mL of 70% Percoll, and centrifuged at 20°C and 800 *g* for 20 minutes with deceleration set to 0. Cells from the interphase were collected, washed once, and then resuspended in supplemented RPMI. For neonatal gut samples, cell suspensions, following digestions, were filtered through 70-μm cell strainers and were then used directly.

Experimental autoimmune encephalomyelitis. EAE was induced by subcutaneous injection of 50 μg of MOG_{35-55} peptide in CFA, while 2 ng pertussis toxin was injected i.p. on the day of immunization and 2 days later. From day 11 after immunization and until day 21, mice were weighed and scored for clinical signs as follows: 0, no symptoms; 1, tail paralysis; 1.5, impaired righting reflex; 2, paralysis of 1 hind limb; 2.5, paralysis of both hind limbs; 3, paralysis of 1 forelimb; 3.5, paralysis of 1 forelimb and weak second forelimb; 4, total limb paralysis.

Mice were euthanized at day 11 or 21 after immunization and were perfused with PBS. LN cells were isolated as described above. Brain tissue was mechanically minced and passed through a 70-μm cell strainer to obtain a single-cell suspension. Lymphocytes were separated using density gradient centrifugation with 47% Percoll (GE Healthcare), layered on 4 mL of 70% Percoll, and centrifuged at 20°C and 900 *g* for 30 minutes with deceleration set to 0.

In vitro stimulation of lymphocytes. For LN lymphocytes, 10^7 cells were cultured for 3.5 hours in the presence of 50 ng/mL PMA (MilliporeSigma), 750 ng/mL ionomycin (MilliporeSigma), and 1 μL/mL BD GolgiStop (containing monensin). Single-cell suspensions from intestinal lamina propria were stimulated with 40 ng/mL of IL-23 (R&D Systems) for 3 hours followed by 50 ng/mL PMA, 750 ng/mL ionomycin, and 1 μL/mL BD GolgiStop for an additional 3 hours.

Flow cytometry. Cells were harvested by centrifugation at 400 *g* for 5 minutes at 4°C followed by staining with fixable viability stain (BD Horizon FVS700) for 10 minutes on ice in PBS. Subsequently, surface antigens were stained in FACS buffer for 30 minutes on ice. For cytokine staining, cells were then fixed and permeabilized by incubation in BD Fix/Perm solution for 15 minutes at room temperature followed by washing once in BD Perm/Wash solution. Intracellular cytokines were stained in BD Perm/Wash for 15 minutes at room temperature. For transcription factor staining, after surface staining, the cells were fixed using the Fixation/Permeabilization buffer in the BD Transcription Factor kit for 45 minutes at 4°C. Transcription factors were stained in permeabilization buffer from the same kit for 45 minutes at 4°C. Conversely, for combined transcription factor and cytokine staining, after surface staining, the cells were fixed using the Fixation/Permeabilization buffer in the FoxP3 transcription factor staining kit (eBioscience) for 1 hour at 4°C. Cytokines and transcription factors were then stained in the permeabilization buffer from the same kit following the manufacturer's guidelines.

All antibodies were used at a 1:200 dilution unless otherwise specified. Antibodies used herein were as follows: CD4-FITC (RM4-4; BD Biosciences), CD19-FITC (6D5; BioLegend), TCRβ-APCeF780 (H57-597; eBioscience), TCRγδ-BV421 (GL3; BD Biosciences), CD45-V500 (30-F11; BD Biosciences), CD3-PECF594 (BM10-37; BD Biosciences), RORγt-APC (B2D; BD Biosciences), IL-17–BV786 (TC11-18H10; BD Biosciences), IL-22–PE (1H8PWSR; eBioscience), T-bet–PE-Cy7 (4B10; BioLegend), IFN-γ–PerCP-Cy5.5 (XMG1.2; BD Biosciences), CD69-V450 and Pe-CF594 (H1.2F3; BD Biosciences), CCR6–Alexa Fluor 647 (140706; BD Biosciences), CD27–PE-Cy7 (LG.3A10; BD Biosciences), CD44-V500 (1M7; BD Biosciences), and Ki67-BV786 (B56; BD Biosciences; 1:100). For Vγ6 staining, the cells were stained in the antibody mixture containing TCRγδ-BV421 (GL3; BD Biosciences) for 15 minutes on ice, and then the anti-Vγ6 antibody (17D1; rat IgM; 4 μL/test) was added and incubated for an extra 30 minutes on ice. Subsequently, the cells were washed once, and stained with anti-rat IgM-PE (RM-7B4; eBioscience) for 30 minutes on ice. The cells were then washed and analyzed.

To determine the level of p-STAT5, 1×10^6 cells were fixed 100 μL with BD Phosflow Lyse/Fix (diluted to 1× with water) for 10 minutes at 37°C. Subsequently, cells were washed once with FACS buffer and resuspended in 100 μL BD Phosflow Perm Buffer III, which was prechilled to –20°C, and incubated on ice for 30 minutes. Cells were then washed once with FACS buffer and stained for 30 minutes on ice in FACS buffer. Antibodies used in the staining of p-STAT5 were CD4-FITC (GK1.5; BD Biosciences), CD8-APC (53-6.7; BD Biosciences), and p-STAT5–PE-Cy7 (47/Stat5 pY694; BD Biosciences; 5 μL/test). Samples were acquired using BD LSR Fortessa and BD FACSDiva software version 8.0.2.

Bone marrow chimera. $CD45.1^+CD45.2^+$ mice were sublethally irradiated (9 Gy) 1 day before being injected i.v. with 10×10^6 cells of whole bone marrow from $CD45.1^+$ WT and $CD45.2^+$ $ROR\gamma t^{CRE}$-$STAT5^{F/F}$ mice mixed at 1:1 ratio. All chimeras were analyzed 12–14 weeks after reconstitution.

Transfer of neonatal γδ T cells in Rag1$^{-/-}$ *mice*. Thymi from newborn $CD45.1^+$ and $ROR\gamma t^{CRE}$-$STAT5^{F/F}$ mice (1 day old) were dissected, and total thymocytes were prepared as mentioned above. Subsequently, γδ T cells were enriched by depletion of $CD4^+$ and $CD8^+$ T cells as follows: the isolated thymocytes were resuspended at a concentration of 1×10^8 cells/mL in MACS buffer and incubated for 10 minutes at room temperature with biotinylated anti-CD4 (GK1.5; BioLegend), anti-CD8 (53-6.7; BioLegend), and anti-TCRβ (H57-597; BioLegend) at a concentration of 1:200 and 50 μL/mL normal rat serum. Subsequently, 75 μL/mL of EasySep Streptavidin RapidSpheres were added and incubated for 2.5 minutes at room temperature. Finally, the mixture was incubated for 2.5 minutes in an EasySep magnet, and negative fraction was collected. The enriched γδ T cells from $ROR\gamma t^{CRE}$-$STAT5^{F/F}$ mice were then mixed at 1:1 ratio with γδ T cells from $CD45.1^+$ mice. Approximately 2×10^5 mixed cells were injected i.v. in adult *Rag1*$^{-/-}$ recipients. Reconstitution of γδ T cells in the LNs of *Rag1*$^{-/-}$ recipients was analyzed 3 weeks after transfer.

Antibiotics administration. Pregnant female mice were treated with a cocktail of the following antibiotics: 1 mg/mL colistin, 5 mg/mL streptomycin, 1 mg/mL ampicillin, and 0.5 mg/mL vancomycin (all antibiotics from MilliporeSigma) in their drinking water starting 3 days before delivery and until weaning of pups (3 weeks after the birth). The antibiotic-containing drinking water was replaced once a week until analysis.

Citrobacter infection. *Citrobacter rodentium* strain DBS100 (ATCC 51459; American Type Culture Collection) was purchased from ATCC and was cultured in Luria-Bertani broth overnight. Colony-forming units per milliliter were determined by measurement of the OD at 600 nm. Pups that were 10–12 days old were infected by oral gavage of 5×10^6 CFU per mouse in a volume of 50 μL. At day 6 after infection, the pups were euthanized, and colons and fecal samples were collected. Bacterial load in the feces was determined as previously described (65).

Cell sorting, RNA extraction, cDNA synthesis, and real-time PCR. Stained cells from thymi of 1-day-old pups or from LNs of adult mice were sorted using BD FACSAria Fusion and BD FACSDiva software version 8.0.2. Target populations were sorted directly in RLT buffer (Qiagen) supplemented with 2-mercaptoethanol. Total RNA was extracted using an RNeasy Micro Kit (Qiagen) and then used for cDNA synthesis using an iScript cDNA synthesis kit (Bio-Rad), according to the manufacturer's protocol. SsoFast EvaGreen Supermix (Bio-Rad) was used to catalyze real-time PCR reactions, which were run on CFX96 (Bio-Rad) and analyzed using Bio-Rad CFX manager software. Gene expression levels were normalized to that of β-actin. The following primers were used: *Actb*, forward 5′-GGCTGTATTCCCCTCCATCG-3′, reverse 5′-CCAGTTGGTAACAATGCCATGT-3′; *Stat5a*, forward 5′-TCCGCAGCACCAGGTAAA-3′, reverse 5′-GGGATTATCCAAGTCAATAGCATC-3′; *Stat5b*, forward 5′-ACAACGGCAGCTCTCCAG-3′, reverse 5′-TGGGCAAACTGAGCTTGGATC-3′;

Ccr2, forward 5′-ATCCACGGCATACTATCAACATC-3′, reverse 5′-CAAGGCTCACCATCATCGTAG-3′; *Csf2*, forward 5′-GGCCTTGGAAGCATGTAGAGG-3′, reverse 5′-GGAGAACTCGTTAGAGACGACTT-3′; *Cd163l1*, forward 5′-CTGGCCTCTGAGTTTAGGGTC-3′, reverse 5′-CCCTTGGTGTCGAACCAGC-3′; *Il2ra,* forward 5′-AACCATAGTACCCAGTTGTCGG-3′, reverse 5′-TCCTAAGCAACGCATATAGACCA-3′; *Fasl*, forward 5′-TCCGTGAGTTCACCAACCAAA-3′, reverse 5′-GGGGGTTCCCTGTTAAATGGG-3′; *Apobec2*, forward 5′-GATCTTCCGCCCTTCGAGATT-3′, reverse 5′-TCTGTACTTCGACCACATAGCA-3′; *Il18r1*, forward 5′-ACTTTTGCTGTGGAGACGTTAC-3′, reverse 5′-CCGGCTTTTCTCTATCAGTGAAT-3′; *Bcl2*, forward 5′-GTCGCTACCGTCGTGACTTC-3′, reverse 5′-CAGACATGCACCTACCCAGC-3′; *Tnfsf8*, forward 5′-GCACAAGTCGCAGCTACTTCT-3′, reverse 5′-GGAGTGGAGTCCTTTTTCTGG-3′; *Nfil3*, forward 5′-GAACTCTGCCTTAGCTGAGGT-3′, reverse 5′-ATTCCCGTTTTCTCCGACACG-3′.

Statistics. Flow cytometry data were analyzed using FlowJo version 10 software (BD Biosciences). All statistical analyses and graphs were generated using GraphPad Prism version 7. All statistical tests used are described in the figure legends. We used the nonparametric Mann-Whitney test. EAE data were analyzed with 2-way ANOVA with Bonferroni's multiple-comparisons test.

Study approval. All animal breeding and experiments were performed in-house at the Technical University of Denmark and only after approval from the Danish Animal Experiments Inspectorate (Copenhagen, Denmark).

Author contributions

VB designed the study, oversaw all work, performed experiments, and wrote the manuscript. DK, RA, and JR designed and performed experiments, analyzed data, and helped write the manuscript. MTV performed experiments. HAN, TS, BM, and RM generated the STAT5 GOF mutant strains, performed experiments, analyzed data, and helped write the manuscript. EMC and AT performed and analyzed experiments. The authorship order of the equally contributing authors reflects the chronology at which they got involved in this work.

Acknowledgments

We thank John O'Shea (NIH/National Institute of Arthritis and Musculoskeletal and Skin Diseases, Bethesda, Maryland, USA) and Stephen Shoenberger (La Jolla Institute for Immunology, La Jolla, California, USA) for critically reading the manuscript and Immo Prinz (University of Hanover, Hanover, Germany) for providing us with the Vγ6 antibody (17D1). This work, and VB and DK specifically, were supported by Lundbeck Foundation grant R163-2013-15201. DK was additionally supported by LEO Foundation grant LF16020. JR and RA were supported by Technical University of Denmark PhD scholarships. RM, HAN, TS, and BM were supported by the Austrian Science Fund (FWF) (SFB-F04707, SFB-F06105, and under the frame of ERA PerMed [I 4218-B] and ERA-NET [I 4157-B]). RM and HAN were also generously supported by a private cancer metabolism grant donation from Liechtenstein. EMC was supported by a Natural Sciences and Engineering Research Council of Canada (NSERC) Discovery grant. EMC holds the Lawson Family Chair in Microbiome Nutrition Research at the University of Toronto.

Address correspondence to: Vasileios Bekiaris, Department of Health Technology, Technical University of Denmark, Kemitorvet, Building 202, 2800 Kongens Lyngby, Denmark. Phone: 459.351.1297; Email: vasbek@dtu.dk.

1. Conti HR, et al. Oral-resident natural Th17 cells and γδ T cells control opportunistic Candida albicans infections. *J Exp Med*. 2014;211(10):2075–2084.
2. Cho JS, et al. IL-17 is essential for host defense against cutaneous Staphylococcus aureus infection in mice. *J Clin Invest*. 2010;120(5):1762–1773.
3. Sutton CE, Lalor SJ, Sweeney CM, Brereton CF, Lavelle EC, Mills KH. Interleukin-1 and IL-23 induce innate IL-17 production from gammadelta T cells, amplifying Th17 responses and autoimmunity. *Immunity*. 2009;31(2):331–341.
4. Michel ML, Pang DJ, Haque SF, Potocnik AJ, Pennington DJ, Hayday AC. Interleukin 7 (IL-7) selectively promotes mouse and human IL-17-producing γδ cells. *Proc Natl Acad Sci U S A*. 2012;109(43):17549–17554.
5. Bekiaris V, Šedý JR, Macauley MG, Rhode-Kurnow A, Ware CF. The inhibitory receptor BTLA controls γδ T cell homeostasis and inflammatory responses. *Immunity*. 2013;39(6):1082–1094.
6. Wu P, et al. γδT17 cells promote the accumulation and expansion of myeloid-derived suppressor cells in human colorectal cancer. *Immunity*. 2014;40(5):785–800.
7. Coffelt SB, et al. IL-17-producing γδ T cells and neutrophils conspire to promote breast cancer metastasis. *Nature*. 2015;522(7556):345–348.
8. Cai Y, et al. Pivotal role of dermal IL-17-producing γδ T cells in skin inflammation. *Immunity*. 2011;35(4):596–610.
9. Turchinovich G, Hayday AC. Skint-1 identifies a common molecular mechanism for the development of interferon-γ-secreting versus interleukin-17-secreting γδ T cells. *Immunity*. 2011;35(1):59–68.
10. Malhotra N, et al. A network of high-mobility group box transcription factors programs innate interleukin-17 production. *Immunity*. 2013;38(4):681–693.
11. Zuberbuehler MK, et al. The transcription factor c-Maf is essential for the commitment of IL-17-producing γδ T cells. *Nat Immunol*. 2019;20(1):73–85.
12. Wencker M, et al. Innate-like T cells straddle innate and adaptive immunity by altering antigen-receptor responsiveness. *Nat Immunol*. 2014;15(1):80–87.
13. Muñoz-Ruiz M, et al. TCR signal strength controls thymic differentiation of discrete proinflammatory γδ T cell subsets. *Nat Immunol*. 2016;17(6):721–727.
14. Sumaria N, Grandjean CL, Silva-Santos B, Pennington DJ. Strong TCRγδ signaling prohibits thymic development of IL-17A-secreting γδ T cells. *Cell Rep*. 2017;19(12):2469–2476.
15. Spidale NA, et al. Interleukin-17-producing γδ T cells originate from SOX13^{+} progenitors that are independent of γδTCR signaling. *Immunity*. 2018;49(5):857–872.e5.
16. Haas JD, et al. Development of interleukin-17-producing γδ T cells is restricted to a functional embryonic wave. *Immunity*. 2012;37(1):48–59.
17. Cai Y, et al. Differential developmental requirement and peripheral regulation for dermal Vγ4 and Vγ6T17 cells in health and inflammation. *Nat Commun*. 2014;5:3986.
18. Stark GR, Darnell JE. The JAK-STAT pathway at twenty. *Immunity*. 2012;36(4):503–514.
19. Villarino A, et al. Signal transducer and activator of transcription 5 (STAT5) paralog dose governs T cell effector and regulatory functions. *Elife*. 2016;5:e08384.
20. de Araujo ED, et al. Structural and functional consequences of the STAT5B^{N642H} driver mutation. *Nat Commun*. 2019;10(1):2517.
21. Hoelbl A, et al. Clarifying the role of Stat5 in lymphoid development and Abelson-induced transformation. *Blood*. 2006;107(12):4898–4906.
22. Yao Z, et al. Nonredundant roles for Stat5a/b in directly regulating Foxp3. *Blood*. 2007;109(10):4368–4375.
23. Yao Z, et al. Stat5a/b are essential for normal lymphoid development and differentiation. *Proc Natl Acad Sci U S A*. 2006;103(4):1000–1005.
24. Imada K, et al. Stat5b is essential for natural killer cell-mediated proliferation and cytolytic activity. *J Exp Med*. 1998;188(11):2067–2074.

25. Villarino AV, et al. Subset- and tissue-defined STAT5 thresholds control homeostasis and function of innate lymphoid cells. *J Exp Med*. 2017;214(10):2999–3014.
26. Wagatsuma K, et al. STAT5 orchestrates local epigenetic changes for chromatin accessibility and rearrangements by direct binding to the TCRγ locus. *J Immunol*. 2015;195(4):1804–1814.
27. Cohen AC, et al. Cutting edge: Decreased accumulation and regulatory function of CD4$^+$ CD25(high) T cells in human STAT5b deficiency. *J Immunol*. 2006;177(5):2770–2774.
28. Kanai T, Jenks J, Nadeau KC. The STAT5b pathway defect and autoimmunity. *Front Immunol*. 2012;3:234.
29. Hwa V. STAT5B deficiency: impacts on human growth and immunity. *Growth Horm IGF Res*. 2016;28:16–20.
30. Pham HTT, et al. STAT5BN642H is a driver mutation for T cell neoplasia. *J Clin Invest*. 2018;128(1):387–401.
31. Cross NCP, et al. Recurrent activating STAT5B N642H mutation in myeloid neoplasms with eosinophilia. *Leukemia*. 2019;33(2):415–425.
32. Ma CA, et al. Somatic STAT5b gain-of-function mutations in early onset nonclonal eosinophilia, urticaria, dermatitis, and diarrhea. *Blood*. 2017;129(5):650–653.
33. Rajala HL, et al. Discovery of somatic STAT5b mutations in large granular lymphocytic leukemia. *Blood*. 2013;121(22):4541–4550.
34. Bandapalli OR, et al. The activating STAT5B N642H mutation is a common abnormality in pediatric T-cell acute lymphoblastic leukemia and confers a higher risk of relapse. *Haematologica*. 2014;99(10):e188–e192.
35. Nicolae A, et al. Frequent STAT5B mutations in γδ hepatosplenic T-cell lymphomas. *Leukemia*. 2014;28(11):2244–2248.
36. Nairismägi ML, et al. JAK-STAT and G-protein-coupled receptor signaling pathways are frequently altered in epitheliotropic intestinal T-cell lymphoma. *Leukemia*. 2016;30(6):1311–1319.
37. Küçük C, et al. Activating mutations of STAT5B and STAT3 in lymphomas derived from γδ-T or NK cells. *Nat Commun*. 2015;6:6025.
38. Eberl G, Littman DR. Thymic origin of intestinal alphabeta T cells revealed by fate mapping of RORγt$^+$ cells. *Science*. 2004;305(5681):248–251.
39. Cui Y, et al. Inactivation of Stat5 in mouse mammary epithelium during pregnancy reveals distinct functions in cell proliferation, survival, and differentiation. *Mol Cell Biol*. 2004;24(18):8037–8047.
40. Heilig JS, Tonegawa S. Diversity of murine gamma genes and expression in fetal and adult T lymphocytes. *Nature*. 1986;322(6082):836–840.
41. Agerholm R, Rizk J, Viñals MT, Bekiaris V. STAT3 but not STAT4 is critical for γδT17 cell responses and skin inflammation. *EMBO Rep*. 2019;20(11):e48647.
42. Laurence A, et al. Interleukin-2 signaling via STAT5 constrains T helper 17 cell generation. *Immunity*. 2007;26(3):371–381.
43. Tripathi P, et al. STAT5 is critical to maintain effector CD8+ T cell responses. *J Immunol*. 2010;185(4):2116–2124.
44. Maurer B, et al. High activation of STAT5A drives peripheral T-cell lymphoma and leukemia. *Haematologica*. 2020;105(2):435–447.
45. Onishi M, et al. Identification and characterization of a constitutively active STAT5 mutant that promotes cell proliferation. *Mol Cell Biol*. 1998;18(7):3871–3879.
46. Petermann F, et al. γδ T cells enhance autoimmunity by restraining regulatory T cell responses via an interleukin-23-dependent mechanism. *Immunity*. 2010;33(3):351–363.
47. Papotto PH, et al. IL-23 drives differentiation of peripheral γδ17 T cells from adult bone marrow-derived precursors. *EMBO Rep*. 2017;18(11):1957–1967.
48. Sheridan BS, et al. γδ T cells exhibit multifunctional and protective memory in intestinal tissues. *Immunity*. 2013;39(1):184–195.
49. Sutherland TE, et al. Chitinase-like proteins promote IL-17-mediated neutrophilia in a tradeoff between nematode killing and host damage. *Nat Immunol*. 2014;15(12):1116–1125.
50. Brown CC, et al. Retinoic acid is essential for Th1 cell lineage stability and prevents transition to a Th17 cell program. *Immunity*. 2015;42(3):499–511.
51. Rajaii F, Bitzer ZT, Xu Q, Sockanathan S. Expression of the dominant negative retinoid receptor, RAR403, alters telencephalic progenitor proliferation, survival, and cell fate specification. *Dev Biol*. 2008;316(2):371–382.
52. Rani A, Murphy JJ. STAT5 in cancer and immunity. *J Interferon Cytokine Res*. 2016;36(4):226–237.
53. Kofoed EM, et al. Growth hormone insensitivity associated with a STAT5b mutation. *N Engl J Med*. 2003;349(12):1139–1147.
54. Al Nabhani Z, et al. A weaning reaction to microbiota is required for resistance to immunopathologies in the adult. *Immunity*. 2019;50(5):1276–1288.e5.
55. Torow N, Hornef MW. The neonatal window of opportunity: setting the stage for life-long host-microbial interaction and immune homeostasis. *J Immunol*. 2017;198(2):557–563.
56. Haricharan S, Li Y. STAT signaling in mammary gland differentiation, cell survival and tumorigenesis. *Mol Cell Endocrinol*. 2014;382(1):560–569.
57. Papotto PH, Ribot JC, Silva-Santos B. IL-17$^+$ γδ T cells as kick-starters of inflammation. *Nat Immunol*. 2017;18(6):604–611.
58. Sandrock I, et al. Genetic models reveal origin, persistence and non-redundant functions of IL-17-producing γδ T cells. *J Exp Med*. 2018;215(12):3006–3018.
59. Hirano M, et al. Evolutionary implications of a third lymphocyte lineage in lampreys. *Nature*. 2013;501(7467):435–438.
60. Loh CY, Arya A, Naema AF, Wong WF, Sethi G, Looi CY. Signal transducer and activator of transcription (STATs) proteins in cancer and inflammation: functions and therapeutic implication. *Front Oncol*. 2019;9:48.
61. Vainchenker W, Leroy E, Gilles L, Marty C, Plo I, Constantinescu SN. JAK inhibitors for the treatment of myeloproliferative neoplasms and other disorders. *F1000Res*. 2018;7:82.
62. Chitadze G, Oberg HH, Wesch D, Kabelitz D. The ambiguous role of γδ T lymphocytes in antitumor immunity. *Trends Immunol*. 2017;38(9):668–678.
63. Lochner M, et al. In vivo equilibrium of proinflammatory IL-17$^+$ and regulatory IL-10$^+$ Foxp3$^+$ RORγt$^+$ T cells. *J Exp Med*. 2008;205(6):1381–1393.
64. Yu F, Sharma S, Edwards J, Feigenbaum L, Zhu J. Dynamic expression of transcription factors T-bet and GATA-3 by regulatory T cells maintains immunotolerance. *Nat Immunol*. 2015;16(2):197–206.
65. Sagaidak S, Taibi A, Wen B, Comelli EM. Development of a real-time PCR assay for quantification of Citrobacter rodentium. *J Microbiol Methods*. 2016;126:76–77.